Bulletin of the Seismological Society of America, 91, 6, pp. 1417–1432, December 2001

Paleoseismologic Evidence for a Very Large (M_w >7), Post-A.D. 1660 Surface Rupture on the Eastern San Cayetano Fault, Ventura County, California: Was This the Elusive Source of the Damaging 21 December 1812 Earthquake?

by James F. Dolan and Thomas K. Rockwell

Abstract The first paleoseismologic data from the San Cayetano fault, a major reverse fault that extends along the northern edge of the Ventura Basin northwest of Los Angeles, reveal that the most recent event on the eastern part of the fault generated at least 4.3 m of surface slip. Age determinations from detrital charcoal recovered from the faulted section indicate that this surface rupture occurred after A.D. 1660; the faulted deposits are overlain by unfaulted historical alluvium containing abundant metal fragments and a leather glove. Comparison of the large surface slip in this event with data from other earthquakes indicates that the most recent eastern San Cayetano surface rupture was larger than M_w 7 and was probably of the order of magnitude 7.5—much larger than any earthquakes that have occurred on Los Angeles metropolitan region faults during the past 150 yr. Such a large event almost certainly would have been recorded had it occurred during the historical period, even if it had occurred during the earliest part of the historical era between ca. A.D. 1780 and 1850. Although this surface rupture could have occurred during the century immediately preceding the historic era, the location and large size of the event lead us to suggest that the trench exposed evidence for the damaging earthquake of 21 December 1812. Whether the most recent surface rupture on the eastern San Cayetano fault was the 21 December 1812 event, these paleoseismologic data add to a growing body of evidence that shows that large earthquakes have occurred on faults within and adjacent to the Los Angeles metropolitan region, reemphasizing the need to include such large events on urban faults in future seismic hazard analyses of the region.

Introduction

The San Cayetano fault is a major, north-dipping reverse fault that extends for 40 km along the northern edge of the Ventura Basin northwest of Los Angeles and westward into the mountains west of Fillmore (Fig. 1). The fault has been mapped in detail both at the surface and in the subsurface by a number of researchers, including Schleuter (1976), Çemen (1977, 1989), Dibblee (1987, 1990a,b, 1991), Rockwell (1988), and Huftile and Yeats (1995a,b, 1996). These studies reveal that the San Cayetano fault is separated into two major sections (or lobes) by a sharply defined, 4-km-wide right step along Sespe Creek near the city of Fillmore (Fig. 1). The eastern, or Modelo lobe (so named because of prominent exposures of the Miocene Modelo Formation in the hanging wall), reaches the surface near the southern edge of the mountain front (Figs. 2 and 3). The surface trace of the San Cayetano fault dies out several kilometers east of the city of Piru, and the details of the manner in which reverse slip is transferred on to the Santa Susana fault—the major, high-slip-rate, north-dipping reverse fault to the east of the San Cayetano fault—remain unclear. The connection between these two faults is a structurally complicated zone of tight to near-isoclinal folding, and there does not appear to be a simple, throughgoing fault connection between these two faults (Yeats, 1987; Yeats *et al.*, 1994; Huftile and Yeats, 1995a).

The western lobe of the San Cayetano fault differs markedly in character from the eastern lobe. The surface trace of the western lobe lies well above the base of the slope of the mountains west of Fillmore, indicative of the fact that the western San Cayetano fault is underlain by the active,

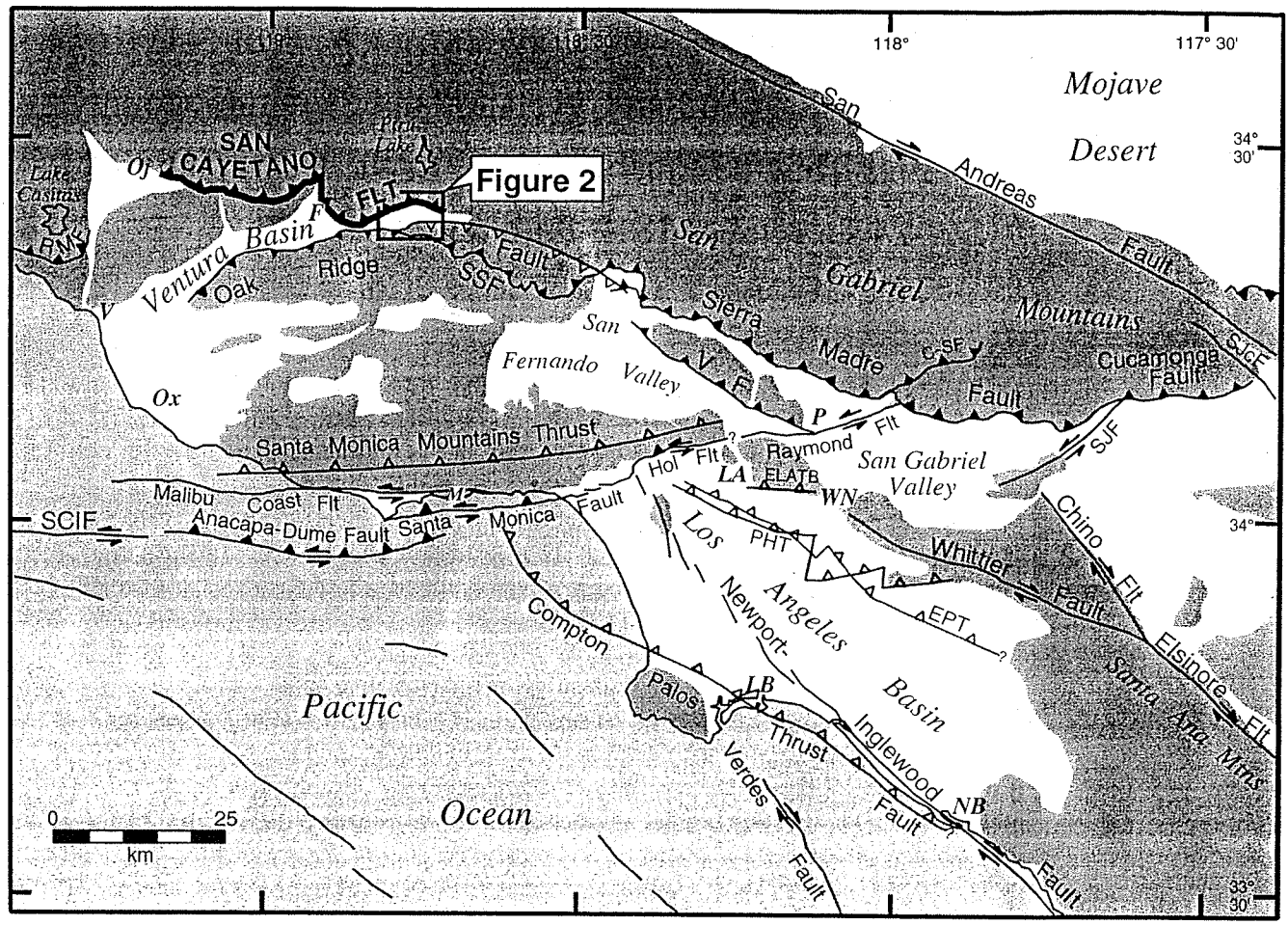

Figure 1. Regional neotectonic map for metropolitan southern California showing major active faults. The San Cayetano fault is a 40-km-long active reverse fault that extends along the northern edge of the Ventura Basin, northwest of the Los Angeles metropolitan region. Fault locations are from Ziony and Jones (1989), Vedder *et al.* (1986), Dolan and Sieh (1992), Sorlien (1994), Shaw and Suppe (1996), Dolan *et al.* (1997, 2000) and Shaw and Shearer (1999). Closed teeth denote reverse fault surface trace; open teeth show upper edge of blind thrust fault ramps. Strike-slip fault surface traces are shown by double arrows. C-SF, Clamshell-Sawpit fault; ELATB, East Los Angeles blind thrust system; EPT, Elysian Park blind thrust fault; Hol Flt, Hollywood fault; PHT, Puente Hills blind thrust fault; RMF, Red Mountain fault; SCIF, Santa Cruz Island fault; SSF, Santa Susana fault; SJcF, San Jacinto fault; SJF, San Jose fault; VF, Verdugo fault; F, Fillmore; LA, Los Angeles; LB, Long Beach; M, Malibu; NB, Newport Beach; Oj, Ojai; Ox, Oxnard; P, Pasadena; V, Ventura; WN, Whittier Narrows. Dark shading denotes mountains. Note location of Figure 2.

south-dipping Sisar blind thrust fault system as well as by a gently north-dipping blind western extension of the San Cayetano fault (Huftile and Yeats, 1995a).

Global Positioning System (GPS) geodetic studies of the Ventura Basin indicate that the basin is shortening in a north–south direction at a rate of approximately 6–7 mm/yr (Donnellan *et al.*, 1993a,b; Argus *et al.*, 1999). This shortening is accommodated along the San Cayetano fault together with the south-dipping Oak Ridge fault, which extends along the southern edge of the basin (Fig. 3) (Çemen, 1989; Dibblee, 1990a, 1991; Suppe and Medwedeff, 1990; Yeats, 1993, 2001; Huftile and Yeats, 1995a,b). Structural modeling and analysis of petroleum industry data from the Hopper Canyon oil field 5 km east of Fillmore indicate major Quaternary reverse separation across the San Cayetano fault. Using petroleum industry well and seismic reflection data, Huftile and Yeats (1996) estimated an average reverse-slip rate for the San Cayetano fault over the past ca. 1 Ma of 7.4 ± 3.0 mm/yr (see also discussion in Yeats, 2001). If this average long-term slip rate is reflective of the current slip rate, correction for the 30° dip of the fault would yield a best-estimate north–south shortening rate of approximately 3–7 mm/yr (Huftile and Yeats, 1996). This suggests that more than half of the shortening across the Ventura Basin is now accommodated by the San Cayetano fault in the region of Hopper Canyon, with relatively less shortening accom-

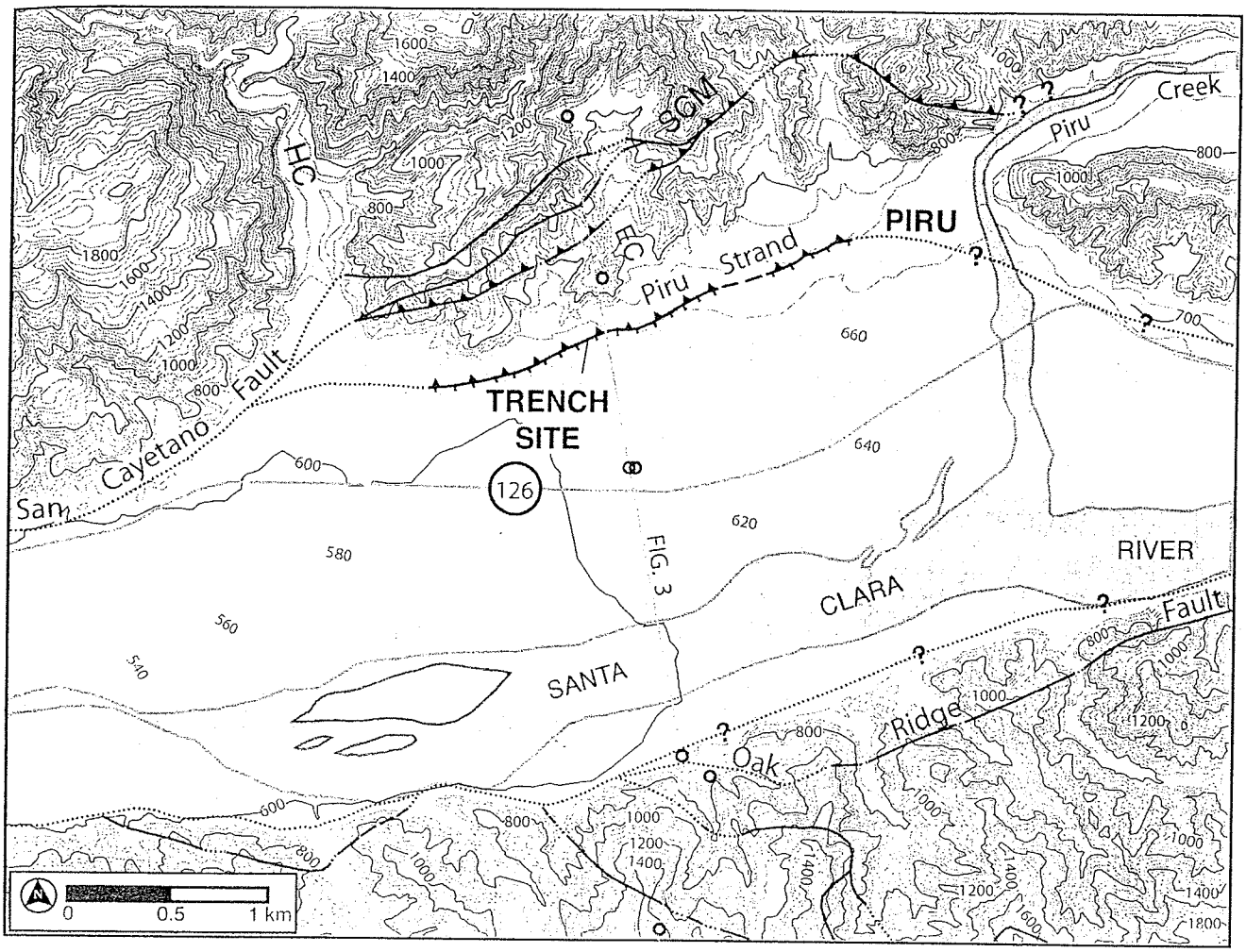

Figure 2. Map of the easternmost 6 km of the San Cayetano fault surface trace near the town of Piru (location in Fig. 1). Note location of our 1999 trench site along the south-facing scarp of Piru strand of the San Cayetano fault (scarps denoted by tick marks on the downhill side). Reverse faults are denoted by closed teeth on the hanging wall. Traces of San Cayetano and Oak Ridge faults are from Dibblee (1991), except as noted. Trace of Piru strand of the San Cayetano fault west of Piru is based on our air photo analysis and field work, following initial identification of these scarps by Çemen (1977, 1989). SCM is main strand of the San Cayetano fault (terminology of Çemen, 1977, 1989; Huftile and Yeats, 1995b), which we suspect may be inactive because this strand exhibits no clear-cut geomorphic evidence of recent activity (see Discussion section). Black open circles show locations of the oil wells used to construct the cross section shown in Figure 3 (Çemen, 1977, 1989; Huftile and Yeats, 1995b). EC, Edwards Canyon; HC, Hopper Canyon. Circled "126" indicates State Highway 126. Buried, northernmost strand of Oak Ridge fault shown near the southeast corner of the figure is based on the observation of apparently uplifted Saugus Formation rocks north of the northernmost trace mapped by Dibblee (1991). Topography digitized from 1952 (photo revised 1988) U.S. Geological Survey 1:24,000 scale Piru 7.5′ Quadrangle. Topographic contour interval is 40′ (12.12 m) in steep terrain; selected 10′ (3.04 m) contours are shown in flatter areas.

modated by reverse slip on the south-dipping thrust fault beneath Oak Ridge on the south side of the Ventura Basin. The very rapid reverse-slip rate for the eastern San Cayetano fault suggests that the San Cayetano fault produces either very large or very frequent earthquakes (or both). Slip rates on the western lobe are slower than on the eastern lobe, ranging from approximately 1.5 to 5.5 mm/yr, dying off to zero where the surface trace of the fault ends just east of the city of Ojai (Fig. 1) (Rockwell, 1988; Huftile and Yeats, 1995a, 1996). This westward decrease in reverse-slip rate may reflect transfer of slip westward onto the Sisar blind thrust system and the blind strand of the San Cayetano fault responsible for uplift of Sulphur Mountain (as originally suggested by Namson and Davis, 1988), and then ultimately

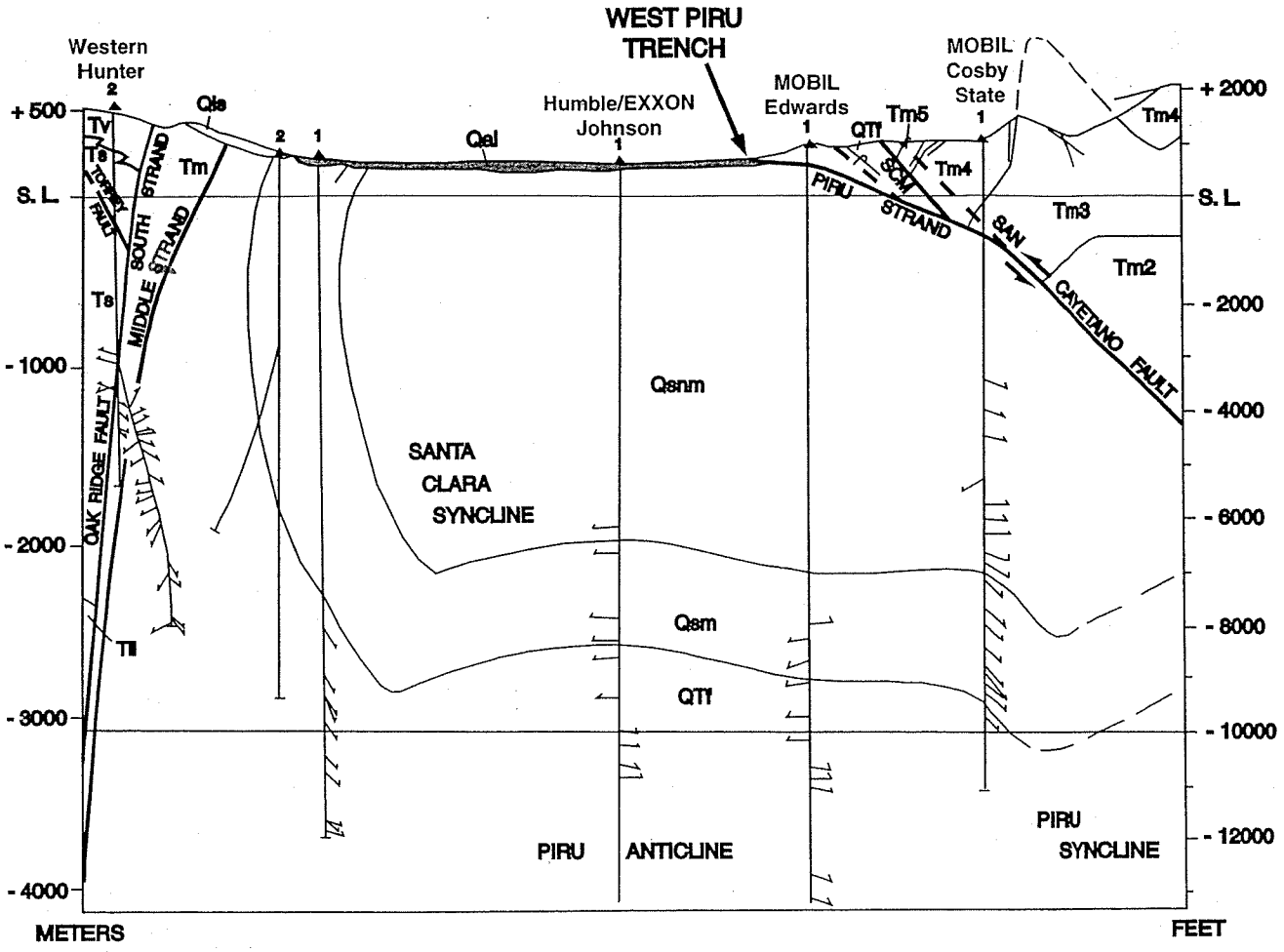

Figure 3. N10W cross section across the east Ventura Basin showing upper part of the San Cayetano fault zone in the vicinity of our 1999 west Piru trench (from Çemen, 1977, 1989; Huftile and Yeats, 1995b). See Figure 2 for location. Thin, vertical lines are oil wells showing dip-meter data. Note near-surface splaying of San Cayetano fault into two distinct strands, the more northerly Main strand of the San Cayetano fault (labeled SCM in the figure) and the southern Piru strand (terminology of Çemen, 1977, 1989; Huftile and Yeats, 1995b). We have modified the cross section to show the Piru strand reaching the surface at our trench exposure, which results in a shallower near-surface dip than that shown in Çemen (1989) and Huftile and Yeats (1995b). Qsm, Quaternary (Pleistocene) Saugus Formation, marine facies; Qsnm, nonmarine facies of Saugus Formation; QTf, Quaternary-Tertiary (Miocene-Pliocene) Towsley Formation; Tml-5, various members of Tertiary (Miocene) Modelo Formation.

onto the north-dipping Red Mountain reverse fault (Huftile and Yeats, 1995a).

Thus, the San Cayetano fault, and in particular the eastern Modelo lobe of the fault, exhibits one of the fastest slip rates of any reverse fault in California, and it may be capable of producing very large earthquakes. Dolan *et al.* (1995) identified the San Cayetano fault as one of six major fault systems within the greater Los Angeles metropolitan region potentially capable of producing $M_w \geq 7.2$ earthquakes. From a seismic hazard standpoint, one of the most critical questions about these faults concerns the size of future earthquakes that they might produce. For example, does the San Cayetano fault rupture in moderate earthquakes in a similar manner as in the 1994 M_w 6.7 Northridge and 1971 M_w 6.7 San Fernando-Sylmar earthquakes? If so, then the fault represents a hazard primarily to the local communities of the rapidly urbanizing Ventura Basin. Alternatively, does the fault rupture in its entirety in $M_w > 7$ events? Such large ruptures would affect a much larger region, including the densely populated San Fernando Valley, the cities of Ventura and Oxnard, and possibly the city of Los Angeles itself. A still more sobering scenario involves the potential for simultaneous rupture of the San Cayetano fault with other north-dipping reverse faults along strike to the east. Rupture of the entire 165-km-long Cucamonga-Sierra Madre-Santa Susana-San Cayetano system could produce a $M_w \geq 7.6$–

7.7 earthquake (Dolan *et al.*, 1995). Such an earthquake could cause catastrophic damage to a very large area encompassing the densely urbanized areas of the Los Angeles and Ventura Basins.

Understanding the past behavior of the San Cayetano fault and the likelihood of a near-future earthquake are critical to assessing the short- and long-term seismic risk to a significant portion of southern California's population. Despite our awareness of the potential hazard posed by the San Cayetano fault, however, prior to this study there were no data available concerning the timing and size of past earthquakes on this fault, other than that the most recent event occurred during late Holocene time on the western lobe of the fault (Rockwell, 1988). In this article we present the first paleoseismologic observations from the San Cayetano fault.

Tectonic Geomorphology of the Eastern San Cayetano Fault

Along the Hopper Canyon-Piru reach of the eastern San Cayetano fault shown in Figure 2, several strands of the fault have been mapped on the basis of bedrock geological relationships and oil-well data (Çemen, 1977, 1989; Dibblee, 1987, 1990a,b, 1991; Huftile and Yeats, 1995a,b). The fault splays upward into two distinct strands at a depth of ca. 500 m (below local ground surface) (Fig. 3) (Çemen, 1977, 1989; Huftile and Yeats, 1995a,b). A set of more northerly, subparallel faults is collectively known as the Main strand (SCM in Figs. 2 and 3) on the basis of evidence of major reverse separations across this strand. The gently dipping, more southerly strand is known as the Piru strand (terminology of Çemen, 1977, 1989). In general, the Main strand juxtaposes different Miocene-Pleistocene bedrock units and extends to the surface in the hills near the southern edge of the mountains north of the Ventura Basin, ca. 100–500 m north of the topographic mountain front. In contrast, the Piru strand extends to the surface across alluvium 100–300 m south of the steep, south-facing mountain front (Fig. 2).

Despite the evidence for kilometers of slip across the Main strand of the San Cayetano fault, this strand does not exhibit any discernible geomorphologic evidence for recent reverse slip. Specifically, if the fault were currently accommodating rapid reverse slip, we would expect the fault trace to be marked by either a pronounced south-facing scarp or some evidence for higher topography along the hanging-wall side of the fault. We observe no such features along the 3-km-long reach of the fault that we examined north and northwest of Piru (Fig. 2). Huftile and Yeats (1995b) reported a possible scarp associated with a strand of the fault that connects with the Main strand in Piru Creek northeast of Piru. But we note that this scarp is subparallel to Piru Creek, and we suggest that it may be fluvial in origin. Whether the scarp reported by Huftile and Yeats (1995b) is tectonic or fluvial in origin, the trace of the Main strand of the San Cayetano fault north and northwest of Piru does not exhibit any topographic expression, such as might be expected along a major, active reverse fault.

In contrast, the Piru strand of the fault exhibits a well-defined, south-facing scarp. This feature was first identified by Çemen (1977, 1989) who described the warping of the alluvial fans south of the mountain front between Piru and Hopper Canyon. The 5- to 8-m-high scarp is traceable nearly continuously west-southwestward for over 2 km from near Piru to the eastern edge of the Hopper Creek drainage, where the scarp has been obscured by recent erosion and deposition along Hopper Creek (Fig. 2). The trend of the scarp projects to the topographic mountain front west of Hopper Creek. Between Piru and Hopper Creek, the scarp extends across several small alluvial fans of differing elevation without a significant change in scarp height. These relations suggested to us that the scarp is of tectonic origin. This interpretation is supported by the fact that active, south-flowing drainages in the area cross the scarp at near right angles. The scarp is marked by abrupt topographic inflection points at its top and base, with the surface slope of the scarp varying from lower than 5° to steeper than 15°, compared with typical alluvial fan slopes of ca. 3°–4° above the scarp and ca. 2°–3° below the scarp.

Given the prominent scarp in young alluvium along the Piru strand, and the absence of clear-cut geomorphic evidence for recent reverse slip along the Main, northern strand of the fault, we concentrated our search for potential paleoseismologic trench sites along the Piru strand. After mapping the Piru strand scarp on aerial photographs, we examined the entire length of the scarp between Hopper Creek and Piru on foot, locating several suitable trench sites.

Trench Results

During August 1999 we excavated a 59-m-long, 4.5-m-deep trench across the prominent scarp of the Piru strand at a site located 2 km west-southwest of the town of Piru and ca. 1.5 km east of Hopper Canyon. We refer to this as the west Piru site. The trench site lies along the western edge of a small alluvial fan that emanates from Edwards Canyon, 500 m to the northeast (Fig. 2). The location of the trench at a site of active alluvial sedimentation led us to expect a relatively complete depositional record. The south-facing scarp at the trench site is located ca. 100 m south of the topographic break in slope at the southern edge of the mountain front. To the east of the trench site, the scarp lies as much as 300 m south of the mountain front (Fig. 2).

Stratigraphy

The trench exposed well-bedded sand, silt, and pebble-cobble gravel layers, many of which could be traced over the length of the trench exposure (Figs. 4–6). All measurements below are in meters south of the north end of the trench, followed by an elevation in meters relative to an arbitrary datum established near the base of the northern end of the trench. For example, the ground surface at the south

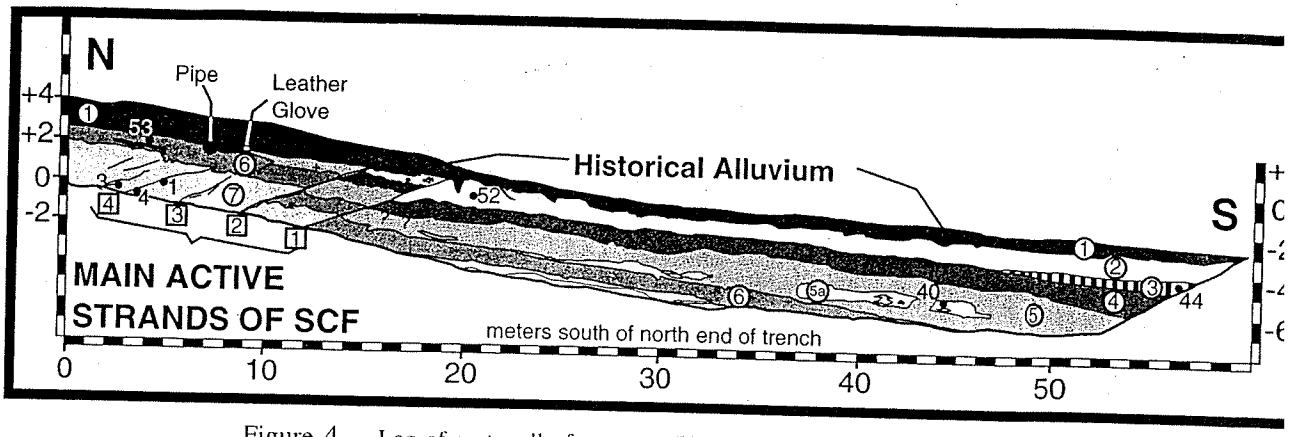

Figure 4. Log of east wall of our west Piru trench. Circled numbers denote the major stratigraphic units discussed in the text. Numbers in square boxes denote four principle fault strands exposed in the trench. Note that strands 1 and 2 accommodated most of the reverse slip during the most recent surface rupture at this site. Small black dots show locations of the detrital charcoal samples from which we obtained ^{14}C age determinations (Table 1). Numbers adjacent to dots correspond to the sample number shown in Table 1. Note that only the sample number is shown on the log; in Table 1 all samples are preceded by the designation SCL which has been omitted from the trench logs for clarity. Horizontal scale is the distance along trench in meters, as measured from the north end of the trench. Vertical scale is meters above or below arbitrary vertical datum near the base of the north end of the trench. No vertical exaggeration.

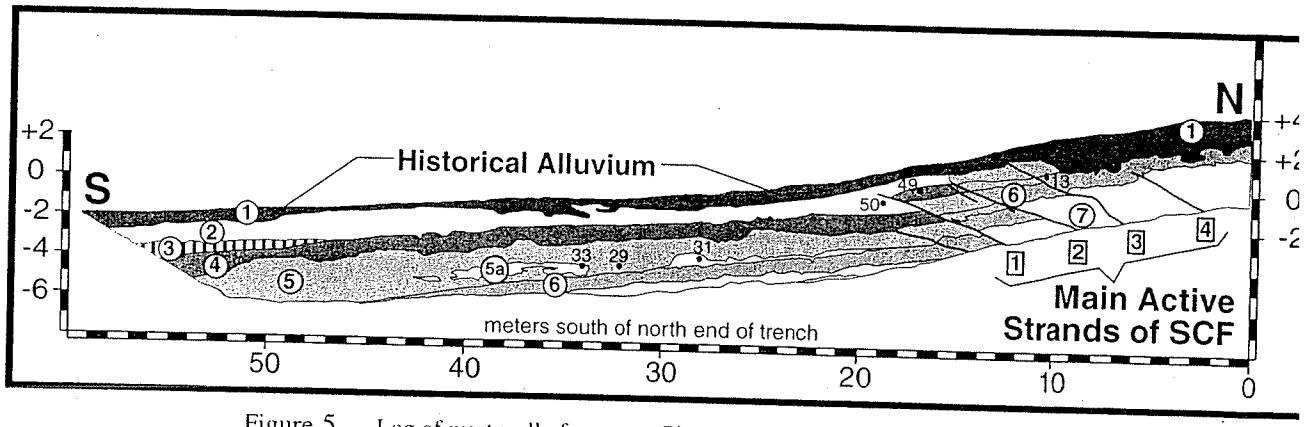

Figure 5. Log of west wall of our west Piru trench. Circled numbers denote major stratigraphic units discussed in the text. Numbers in square boxes denote four principal fault strands exposed in the trench. Small black dots show locations of the detrital charcoal samples from which we obtained ^{14}C age determinations (Table 1). Numbers adjacent to dots correspond to the sample number shown in Table 1. Note that only the sample number is shown on the log; in Table 1 all samples are preceded by the designation SCL. Horizontal scale is the distance along trench in meters, as measured from the north end of the trench. Vertical scale is meters above or below arbitrary vertical datum near the base of the north end of the trench. No vertical exaggeration. North-dipping section of basal contact of Unit 1 at m 10.5; +1.5 m is edge of the historical drainage ditch.

end of the trench, which is located 59.5 m south of the north end of the trench at an elevation of –2.6 m relative to our arbitrary datum, would be noted as m 59.5; –2.6 m.

We encountered seven major stratigraphic units in the trench, referred to as Units 1–7 from youngest to oldest. Unit 1, the youngest unit, consists of predominantly sandy, well-bedded historical alluvium. The historical age of these deposits is demonstrated by the presence of a leather glove near the base of the unit (m 8.8; +1.6 m), by the occurrence c numerous small metal fragments throughout the unit (e.g barbed wire fragments), and by several examples of hori zontal to gently north-dipping terrace levels that were cu into the alluvium during previous development of the orang grove (e.g., m 4.0; +3.5 m and m 11.0; +1.9 m, both o the east wall). The historical Unit 1 alluvium overlies Uni 2 along an irregular, bioturbated gradational contact.

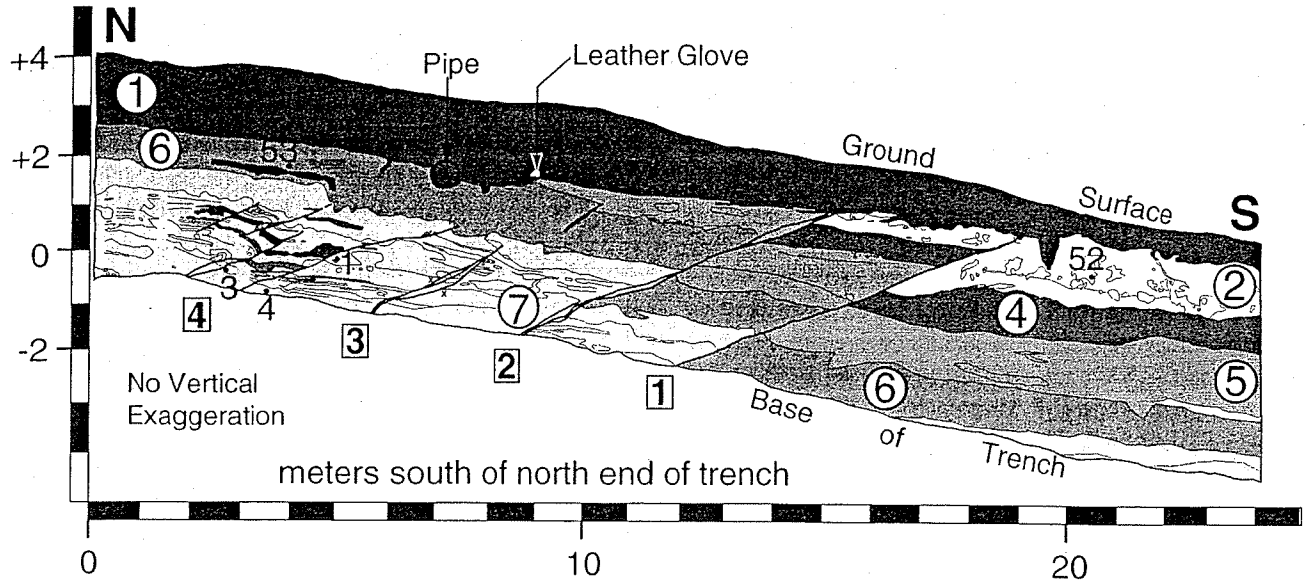

Figure 6. Detail of northern half of east wall of trench. Note the folding of thin gravel layer (black in the figure) and southward thickening of Unit 6 at m 5.0; +1.5 m, which we interpret as possible evidence for the penultimate surface rupture. See Discussion section. Selected marker beds in Unit 7 are shown in black and various shades of gray to illustrate small-scale displacements on strands of fault 4. Numbered small black circles correspond to ^{14}C age determinations for the detrital charcoal samples listed in Table 1. Large circled numbers denote stratigraphic units 1–7. Small x's at m 7; –0.5 m denote displaced top of bed.

Unit 2 is 60–120 cm thick and consists of pale yellow-brown (2.5Y 5/5), friable, fine-grained sand. This unit is continuously exposed from m 18 to the south end of the trench. Unit 2 overlies Units 3 and 4 along a relatively sharp, planar contact.

Unit 3 is a wedge-shaped deposit of pale yellow-olive-brown (2.5Y 4.5/4), densely packed pebble gravel. The unit decreases in thickness from 60 cm at the south edge of the trench to 0 cm where the unit pinches out at m 46.8; +4.4 m. Unit 3 overlies Unit 4 along a sharp, relatively planar contact.

Unit 4 is a medium-brown (10YR 3.5/3) poorly sorted, pebble to large cobble gravel with generally more matrix than Unit 3. The matrix of the Unit 4 gravel is a silty sand. The unit is distinguished by organic enrichment, resulting in its rather dark color, which we interpret as indicating that Unit 4 is a weakly developed, buried paleosol. Unit 4 is of a relatively constant 70- to 100-cm thickness over most of the trench, but thickens gradually to ca. 1.4 m southward from ca. m 48.

Unit 5 is a pale yellow-brown (2.5Y 5.5/4 to 10YR 5.5/5), pebble to small cobble gravel that thickens southward from ca. 75 cm at m 18 to greater than 2 m at the south end of the trench. The unit is distinguished from Unit 4 primarily on the basis of its paler color, a sandier matrix, and a larger percentage of clasts relative to matrix. Unit 5 contains a discontinuous bed of pale yellow-brown sand (Unit 5a) that extends from m 22 to 48. Unit 5a onlaps the base of Unit 5; Unit 5a dips ca. 4° S, more gently than the ca. 9° S dip of the underlying Unit 5/Unit 6 contact. There are no obvious differences between the part of Unit 5 that overlies Unit 5a relative to those parts that underlie Unit 5a. Unit 5 overlies Unit 6 along a sharp, generally planar contact.

Unit 6 is a cohesive, silt to silty fine-grained sand that locally contains ca. 10% disseminated small pebbles. In a few locations (e.g., m 5; +1.9 m, east wall) this medium yellow-brown (10YR 4/4 to 2.5Y 4.5/5) unit is locally well laminated on a centimeter scale. Over most of the trench exposures, however, the unit is massive, suggesting that it has been thoroughly bioturbated. The cohesive nature and darker color of this unit lead us to interpret it as a weakly developed, buried A horizon. Overall, Unit 6 appears to dip slightly more steeply than the overlying units. Unit 6 overlies Unit 7 along a sharp, slightly irregular to planar contact.

Unit 7 is a generally thin-bedded (predominantly 1 to 20 cm thick) sequence of sands and pebble gravels that is more than 2 m thick in the northern 9 m of the trench. Contacts between individual beds are generally sharp, and there is local interfingering among strata. In the southern part of the trench, only the uppermost 50 cm of this unit is exposed between m 16 and 33.

Age Control

The youngest deposit exposed in the trench (Unit 1) contained abundant reworked man-made material (e.g., barbed wire, nails, and other metal fragments). In addition,

we recovered a leather glove from near the base of Unit 1 at m 8.8 on the east wall of the trench, at a burial depth of 1.5 m (Figs. 4 and 6). These observations indicate that Unit 1 is historical. The presence of barbed wire and the leather glove suggests that Unit 1 was probably deposited during the late nineteenth or twentieth centuries.

Accelerator mass spectrometer (AMS) ^{14}C analyses of 13 detrital charcoal samples collected from Units 2–7 indicate that the trench exposed a latest Holocene section. All the detrital charcoal samples received a standard pretreatment consisting of acid/akali/acid washes. The charcoal samples yielded a wide variety of ages, ranging from 163 ± 38 radiocarbon yr B.P. to greater than 44,000 yr B.P. (Figs. 4–7; Table 1). The wide variation of sample ages within the same beds, together with the older-over-younger relationships observed between samples collected from unfaulted stratigraphic sections in the trench, indicates extensive reworking of the detrital charcoal. For example, four samples (SCL-29, -31, -33, and -40) that were recovered from the same stratigraphic level in Units 5 and 5a yielded uncorrected radiocarbon ages of 6629 ± 93, 38,900 ± 1400, 4227 ± 48, and 163 ± 38 yr B.P., respectively (Figs. 4 and 5; Table 1). Three of these samples (SCL-31, -33, and -40) were recovered from the Unit 5a sand, which is enclosed by the textually distinctive gravel of Unit 5, and there was no indication of any recent burrowing that may have introduced these samples. There is no systematic correlation between the ages and sizes of the detrital charcoal samples. We note, however, that the youngest (SCL-13, -40, -44) and oldest (SCL-1, -31, -53) suites of samples yielded the largest amounts of carbon, with samples of intervening age being generally much smaller (Table 1).

Because of the evidence of extensive charcoal reworking in the trench, we are only confident that three of the samples record the approximate burial ages of the units from which they were recovered. Specifically, the aforementioned

Table 1
AMS ^{14}C Dates from Detrital Charcoal Samples*

Unit	Sample #	U of A #	Weight (mg)	$\delta^{13}C$	Trench Grid Location (West Wall)/(East Wall) (m south; m vertical)	^{14}C Age (1-sigma) (Radiocarbon yr B.P.)	Calendric Age Range (2-sigma)	Relative Area under Probability Distribution	
								Period	Area (%)
	SCL-50	AA35901	0.17	−26.9	W 18.50; −0.19	430 ± 85	A.D. 1324–1650	A.D. 1324–1349	2.6
								A.D. 1391–1650	97.4
2	SCL-52	AA35902	0.03	−26.0	E 20.48; −0.51	5,940 ± 460	5716–3805 B.C.	5716–3936 B.C.	99
								3876–3868 B.C.	0.1
								3863–3805 B.C.	0.9
3	SCL-44	AA35899	1.03	−24.2	E 55.90; −4.30	196 ± 41	A.D. 1641–1950*	A.D. 1641–1701	25.4
								A.D. 1722–1815	53
								A.D. 1831–1880	6.5
								A.D. 1915–1950	1.5
14	SCL-49	AA35900	0.04	−26.0	W 16.66; +0.36	2,860 ± 220	1527–419 B.C.	1527–504 B.C.	98.8
								464–419 B.C.	1.2
5	SCL-29	AA35895	0.15	−22.7	W 31.83; −4.16	6,629 ± 93	5719–5382 B.C.	5719–5466 B.C.	95.3
								5445–5420B.C.	2.7
								5401–5382 B.C.	2
5a	SCL-31	AA35896	0.72	−22.5	W 27.68; −3.58	38,900 ± 1,400	Beyond calibration		
5a	SCL-33	AA35897	0.37	−13.0	W 33.77; −4.29	4,227 ± 48	2916–2634 B.C.	2916–2835 B.C.	34
								2819–2663 B.C.	64.2
								2648–2634 B.C.	1.9
5a	SCL-40	AA35898	0.54	−23.7	E 43.85; −5.23	163 ± 38	A.D. 1660–1950‡	A.D. 1660–1709	18.1
								A.D. 1718–1824	48.3
								A.D. 1826–1885	16.3
								A.D. 1912–1950	17.3
6	SCL-13	AA35906	0.54	−25.1	W 10.11; +1.09	323 ± 41	A.D. 1478–1648	A.D. 1478–1648	100
6	SCL-53	AA35903	0.73	−22.9	E 3.81; +1.77	38,900 ± 2,500	Beyond calibration		
7	SCL-1	AA35894	0.51	−23.8	E 4.77; −0.11	<44,448	Beyond calibration		
7	SCL-3	AA35904	0.08	−23.3	E 2.64; −0.31	4,050 ± 180	3080–2038 B.C.	3080–3073 B.C.	0.2
								3027–2116 B.C.	97.9
								2100–2038 B.C.	1.8
7	SCL-4	AA35905	0.15	−24.1	E 3.45; −0.71	27,900 ± 1,700	Beyond calibration		

*Sample locations are shown in Figures 4–7. Note that only the sample numbers are shown in the figures (i.e., the SCL prefix for each sample is omitted for clarity).

†A.D. 1831–1950 age range has been ruled out by historical data. See text for discussion.

‡A.D. 1826–1950 age range has been ruled out by historical data. See text for discussion.

sample SCL-40, recovered from Unit 5 at a burial depth of 4 m, yielded a calibrated, calendric age range of A.D. 1660–1950 (all calendric ages reported in this article are 2-sigma [95% confidence limits] ages calibrated with CALIB 4.3; Stuiver and Reimer, 1993). This age is indistinguishable from the calendric A.D. 1641–1950 age range of sample SCL-44, which was recovered from the Unit 3 gravel wedge 2 m stratigraphically above sample SCL-40 (Fig. 4). The occurrence of sample SCL-40 beneath SCL-44 indicates that Unit 2 cannot be older than about A.D. 1660, narrowing the potential age range of sample SCL-44. The indistinguishable age ranges of samples SCL-40 and -44 indicate that the stratigraphic section encompassing Units 3, 4, and 5 was deposited very rapidly, within at most a few centuries. This inference is consistent with the near absence of any soil development within these strata; development of a weak A/C profile in Unit 4 provides the only evidence for any pedogenesis in Units 2–5. The absence of a discernible cambic (Bw) or calcic (Bk) horizon associated with the buried Unit 4 soil suggests to us that it records only a minimal period of soil development. This weakly developed A/C profile is equivalent to Q2 deposits of Rockwell *et al.* (1985), which are typically less than 500 years in age. Unit 6 exhibits a similar, weakly developed buried A horizon, and thus also probably records a brief period of soil development.

Sample SCL-13, recovered from near the top of Unit 6, yielded a slightly older calendric age range of A.D. 1478–1648. This date is in correct stratigraphic sequence with samples SCL-40 and -44 from the overlying units 5a and 3. Moreover, the ca. 200-yr maximum difference in the ages of Units 6 and 5 suggested by the ^{14}C ages is consistent with the development of the weak A/C soil profile within Unit 6. These age data suggest very rapid deposition of Units 1–6.

The 3080–2038 B.C. calendric age range of sample SCL-3 from near the base of Unit 7 in the northern part of the trench provides a maximum age for this unit. We suspect, however, that Unit 7 may be considerably younger than the maximum possible age provided by the SCL-3 AMS date. Specifically, if the AMS date records the depositional age of the part of Unit 7 from which sample SCL-3 was collected, then the overlying ca. 2 m of Unit 7 would have been deposited over a period of 4000–5000 yr. However, we see no evidence of any significant soil development within Unit 7 that would be consistent with such an extended period of development.

Sample SCL-50, which was recovered from Unit 2 at a burial depth of 1.4 m, yielded a calendric age range of A.D. 1324–1650. This sample is slightly older than the underlying samples SCL-40 and -44, suggesting that SCL-50 has been reworked. Nevertheless, the age of sample SCL-50 confirms that Unit 2 is a latest Holocene deposit, consistent with the lack of a well-developed soil within the upper part of the unit.

Evidence for Faulting

The trench exposed four major fault zones, which we refer to as faults 1–4, from south to north (Figs. 4 and 5). Faults 1 and 2 are both quite planar, and exhibit single shear zones along most of their lengths, with local closely spaced, parallel strands. Displacements along both the southern faults extend up to the same stratigraphic level, at the base of the historical Unit 1 alluvial deposits (Figs. 4–6). Reverse separation across several stratigraphic units is the same at different depths along both faults, suggesting that they have experienced only a single earthquake within the stratigraphic interval exposed in the trench. Moreover, there is no stratigraphic or structural evidence (e.g., colluvial wedges, buried scarps, or truncated faults) that might indicate an earlier surface rupture on faults 1 or 2. In addition, the lack of significant changes in the thicknesses and character of the faulted units across major fault strands suggests that the San Cayetano fault at the trench site experiences near-pure reverse slip, with little to no evidence of significant lateral slip. The apparent across-fault differences in the thicknesses of units 4–6 (e.g., the absence of Unit 4 north of fault 2 and the absence of Units 4 and 5 north of m 9) are caused by the progressive northward-increasing erosion along the base of historical Unit 1 and not by the strike-slip juxtaposition of units of laterally variable thickness.

Fault 1, the southernmost fault, dips 18°–25° and extends from the base of the trench at m 12.4 to the bottom of the historical alluvium at m 18.8. This fault exhibits 160 ± 25 cm of reverse separation, depending on which horizon is used to measure slip. Fault 2, which also dips 18°–25° north, extends from the base of the trench at m 8.6 to the base of the historical alluvium at m 16.1. Fault 2 has accommodated 220 ± 10 cm of reverse slip. Together, faults 1 and 2 have accommodated ca. 4 m of reverse slip.

Fault 3 is a relatively minor strand. Total reverse slip on the fault is less well constrained than for strands 1 and 2, but it is at least 25 cm as measured on the displaced top of Unit 6 on the east wall of the trench. On the west wall of the trench this same contact is separated by 55 ± 5 cm. It is possible that the trench is excavated across a slip transition from fault 3 to another minor strand ca. 1 m structurally above, which appears to have ca. 25 cm of reverse slip as measured on strata within Unit 7. Thus, it is likely that there is ca. 50 cm of reverse slip on fault 3. We therefore assign reverse slip of 50 + 10/–25 cm for fault 3. The dip of fault 3 is ca. 25°, although it is less planar than faults 1 and 2, and locally exhibits dips as steep as 45°. Fault 3 extends from the base of the trench at m 6.4 (east wall)/m 5.5 (west wall) to the base of the historical Unit 1 alluvium-the same stratigraphic level as faults 1 and 2-at m 10.5 (east wall)/m 12.2 (west wall). The upward extension of fault 3 to the base of Unit 1 is best observed on the west wall (Fig. 7) because the upper part of this fault strand becomes somewhat discontinuous on the east wall (Fig. 6). These relationships indicate that fault 3 has a slightly more northeasterly strike than faults 1 and 2. Together, faults 1–3, all of which extend up to the same stratigraphic level at the base of Unit 1, exhibit a total of 430 + 45/–60 cm of reverse separation.

Unlike the single-strand southern faults, fault 4, the

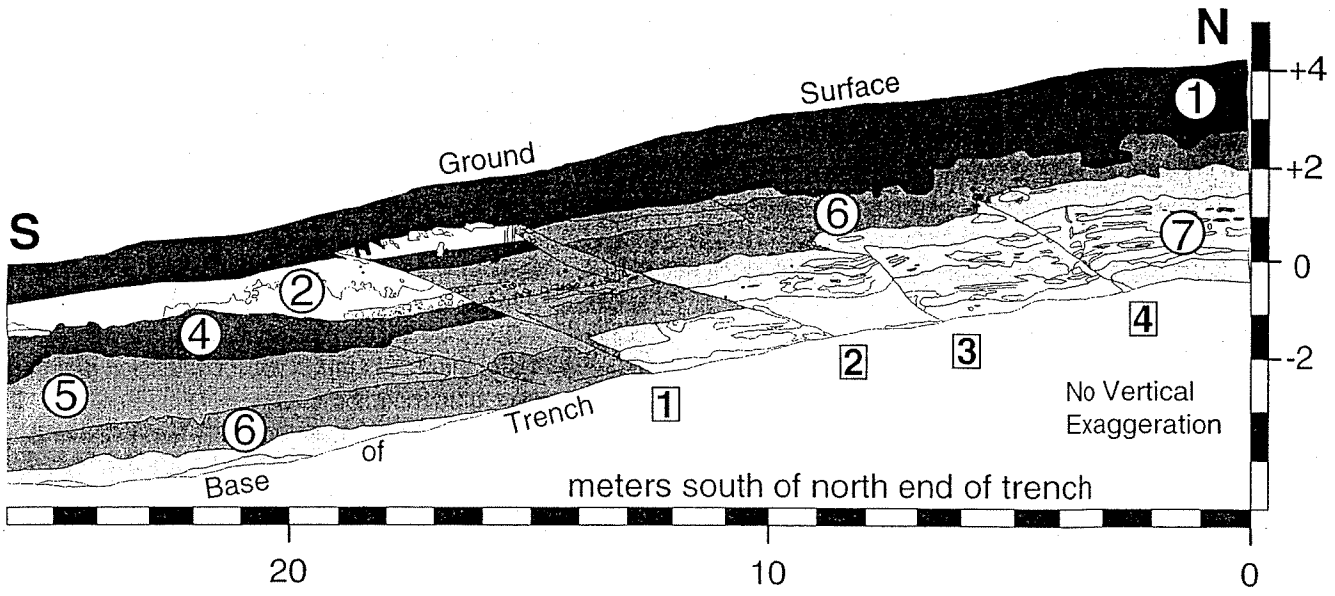

Figure 7. Detail of northern half of west wall of trench. See Discussion section. Numbered triangles correspond to ^{14}C age determinations for the detrital charcoal samples listed in Table 1. Note that the upward termination of fault 3 at the base of historical Unit 1 alluvium is more clearly expressed on this wall than on the eastern trench wall.

northernmost fault, on the east wall consists of a 1.7-m-wide zone of closely spaced minor faults that collectively exhibit ca. 90 ± 10 cm of reverse slip. In the west wall, in contrast, fault 4 exhibits one main strand with a few very minor parallel strands. The exact nature of the upward termination of fault 4 is not as clear as for faults 1–3, because of bioturbation and the presence of a 70-cm-diameter water pipe (m 7; +1.8 m) that extends perpendicular to the trench in the area where the northern fault would project to the surface. Moreover, the northward-increasing amount of erosion of Units 2–6 to the north of fault 1 precludes reconstruction of the prefaulting geometry of these units above fault 4 (Figs. 6 and 7). At issue is whether the northern fault strand terminates at a deeper stratigraphic level than the more southerly faults exposed in the trench. Fault 4 cannot be traced shallower than +1.4 m on the west wall and +1.2 m on the east wall. At m 4.8: +1.4 m on the east wall, a 10-cm-thick pebble gravel layer is warped down to the south at a 90° angle, and the base of Unit 6 deepens by ca. 50 cm across the zone of warping (Fig. 6). It is not clear whether this folding marks the upward termination of fault 4 or whether the fault extends farther upsection, possibly all the way to the same stratigraphic horizon as faults 1–3. It is also possible that fault 4 shallows in dip upward and extends southward as a near-horizontal feature into the massive silty sand of Unit 6.

If fault 4 terminates upward within Unit 6, this would suggest that the penultimate surface rupture along this reach of the San Cayetano fault occurred during or immediately after deposition in Unit 6. Alternatively, the equivocal stratigraphic and structural observations in the trench allow for the possibility that fault 4 may have ruptured up to the same stratigraphic horizon as faults 1–3 (base of Unit 1).

To sum up, although the stratigraphic evidence for the event horizon is not as clear-cut for fault 4 as it is for the southern faults, fault 4 records ca. 90 cm of slip during either the penultimate event or the most recent event. We were unable to excavate any further northward at our trench site because a major water pipe, constructed of easy-to-damage material, extended through the area, and the exact location of the pipe was not known. Thus, we are not sure whether we have excavated all strands of fault 4 (or any more northerly faults). The ca. 90 ± 10 cm of reverse slip on fault zone 4 exposed within the trench is thus a minimum. Although we suspect that fault 4 may record the penultimate surface rupture on the San Cayetano fault, it is equally possible that the reverse slip documented along fault 4 occurred during the most recent event. In this case, the ca. 90 cm of slip on fault 4 would have to be added to the 4.3 m of slip on strands 1–3, for a minimum of greater than or equal to 5.2 m of slip in the most recent surface rupture.

Discussion

The fact that faults 1–3 all terminate at the same very young (historical) stratum at the base of Unit 1, together with the absence of evidence for any extended periods of soil development in the youngest faulted deposits, suggests that faults 1–3 probably record the same surface rupture. This inference is supported by the lack of significant down-dip variation in the total reverse slip on faults 1–3, which strongly suggests that these faults record only a single sur-

face rupture within the stratigraphic interval exposed in the trench. These observations indicate that the most recent surface rupture on the eastern San Cayetano fault occurred after deposition of Unit 2, the youngest faulted stratum, and before deposition of the historical Unit 1 alluvium. Thus, the calendric ages determined for charcoal samples SCL-40 and -44 from the faulted section constrain this earthquake to have occurred after A.D. 1660.

If the deformation associated with fault 4 near the north end of the trench records the penultimate event, then the 3080–2038 B.C. calendric age range of sample SCL-3 from Unit 7 provides a maximum possible age for the penultimate surface rupture. The absence of significant soil development within Unit 7, however, leads us to suspect that the actual age of Unit 7, and therefore the age of the penultimate event, is much younger than the maximum possible age provided by SCL-3. Although it is possible that soils could have been stripped by erosion of Unit 7, it is difficult to completely strip the entire profiles of well-developed soils in such alluvial environments (Rockwell *et al.,* 1985).

Whether the deformation near the north end of the trench records the penultimate event, the minimum amount of reverse slip that occurred on faults 1–3 during the most recent surface rupture at the west Piru site is 430 + 45/–160 cm. As discussed above, the ca. 90 cm of reverse slip recorded on fault 4 may have occurred during the penultimate surface rupture. We reiterate, however, that the stratigraphic data are equivocal regarding this inference, and it is equally possible that the slip on fault 4 occurred during the most recent surface rupture. If so, then the minimum reverse slip at this site during the most recent surface rupture was ca. 520 cm.

Such large displacements are characteristic of moderately large to large earthquakes (Wells and Coppersmith, 1994; Dolan *et al.,* 1995). If the cumulative 4.3 m of reverse slip on faults 1–3 represents the average slip on the fault plane during the most recent event, regressions suggest that the earthquake was about M_w 7.45 ± 0.2 (95% confidence limits for regression on the global data set; Wells and Coppersmith, 1994). If the 4.3 m represents the maximum slip in the event, then it was probably $M_w \sim 7.15 \pm 0.15$ (95% confidence limits; Wells and Coppersmith, 1994). Regressions of displacement on moment magnitude for southern California earthquakes yield similar estimates (Dolan *et al.,* 1995). Thus, the most recent surface rupture on the San Cayetano fault was a large earthquake, almost certainly larger than M_w 7.0 and probably closer to $\sim M_w$ 7.5.

The eastern lobe of the San Cayetano fault, as mapped at the surface, is only ca. 15 km long. A comparison of the regressions of average slip/event on moment magnitude and of rupture area on moment magnitude suggests that the eastern lobe, by itself, is probably too small to generate an earthquake in excess of M_w 7 (Wells and Coppersmith, 1994; Dolan *et al.,* 1995). An assumed 40° north dip for the eastern section of the San Cayetano fault consistent with petroleum industry and seismicity data (Huftile and Yeats, 1996) and a seismogenic thickness of 20 km (Bryant and Jones, 1992) yield a fault plane area of ca. 250 km^2 (Dolan *et al.,* 1995). Failure of a fault plane of this size will typically generate an earthquake of between ca. M_w 6.5 ± 0.25 (Wells and Coppersmith, 1994) and ca. M_w 6.65 ± ~ 0.1 (Dolan *et al.,* 1995). Thus, the most recent surface rupture on the San Cayetano fault almost certainly involved the rupture of faults other than the eastern San Cayetano fault. The most obvious scenario involves simultaneous rupture of both the eastern and the western sections of the San Cayetano fault across the major, 4-km-wide right step in the fault at Sespe Creek near Fillmore. Dolan *et al.* (1995) estimate that rupture of the entire San Cayetano fault would result in a ca. M_w 7.2 event.

This is but one of a number of possible faulting scenarios. Other faulting scenarios include the possibility that the eastern San Cayetano fault ruptured eastward onto the Santa Susana fault. We consider this to be a less likely scenario because of the structural complexity at the intersection of the two faults and the lack of a demonstrated, through-going fault connection in this area. Another possibility, which is more difficult to assess, is that the eastern San Cayetano fault ruptured together with blind thrust faults to the west (Namson and Davis, 1988; Huftile and Yeats, 1995a, 1996).

Does the West Piru Trench Record Evidence of the 21 December 1812 Earthquake?

During December 1812, two large earthquakes struck southern California (Toppozada *et al.,* 1981). The first occurred on 8 December, and was followed 13 days later by a second large event. Jacoby *et al.* (1988) used tree-ring analysis to demonstrate that the 8 December 1812 M_w ca. 7.5 event occurred along the Mojave Desert section of the San Andreas fault (SAF). The causative fault for the 21 December event, however, has not been unequivocally identified, although several previous researchers have suggested an offshore source in the Santa Barbara Channel (see discussion in Toppozada *et al.,* 1981).

Written records from the various Spanish Missions that were scattered across southern California at the time indicate that strong ground shaking occurred over a wide region in the western Transverse Ranges during the 21 December 1812 event (Fig. 7). The following descriptions are taken from Toppozada *et al.* (1981) who conducted a thorough analysis of the historical records for the 1812 earthquakes. Extensive damage occurred at Mission San Buenaventura (modern Ventura), the mission and presidio at Santa Barbara, Mission Santa Inez, and Mission La Purisima Concepcion (modern Lompoc). The severe damage at La Purisima Concepcion, which was probably at least partially the result of local site effects, resulted in the mission being rebuilt elsewhere after the earthquake. It is not clear whether the 21 December event was felt strongly at Mission San Fernando Rey, where strong and repeated earthquakes were reported during December 1812. Although it is possible that the earthquakes recorded at San Fernando included the main-

shock of the 21 December event, it is equally possible that these events were all associated with the 8 December mainshock/aftershock sequence. The 21 December event was apparently not reported at either Mission San Gabriel or at the Pueblo of Los Angeles. The 8 December event was reported in detail from the San Gabriel mission, so the lack of a specific report of the 21 December event probably indicates that the second event was felt much less strongly and/or caused much less damage than the first event. It remains uncertain whether the 21 December 1812 earthquake was strongly felt at the Pueblo of Los Angeles. During this time period, pueblos did not generally issue their own annual reports, and thus it is not surprising that no records from Los Angeles mentioning the 21 December 1812 event have been discovered at the mission archives in Santa Barbara (the source of much of the aforementioned information) (T. Toppozada, 2000, personal comm.). It is possible that the 21 December earthquake was strongly felt as far east as the San Bernardino Valley (Toppozada *et al.*, 1981), although it is also possible that this strong ground shaking was related to the 8 December 1812 earthquake which occurred less than 30 km to the northwest on the SAF (Fig. 8).

The mission records indicate that the 21 December earthquake was actually two strong earthquakes separated by about 15 min (Toppozada *et al.*, 1981). These two events were clearly felt as separate shocks at La Purisima, Santa Inez, and Santa Barbara, and they may have been recorded as two of the "three horrible tremors . . . " that struck Mission San Buenaventura during December 1812. The commander of the presidio at Santa Barbara reported that "there occurred at this Fort two horrible earthquakes between which no notable difference could be discerned beside the fact that they were a quarter of an hour apart" (Arguello, 28 December 1812) (cited in Toppozada *et al.*, 1981, p. 138). Thus, as noted by Toppozada *et al.* (1981), the two 21 December events appear to have been approximately the same size and duration.

As described previously, the paleoseismologic data from the west Piru trench indicate that a very large surface rupture (M_w >7) occurred at that site sometime after A.D. 1660. Such a large event would almost certainly have been recorded had it occurred during the historical period, even if it occurred during the earliest part of the historical era between ca. A.D. 1780 and 1800, the time by which several Spanish missions and towns had been established in the region. The 21 December 1812 event is the only historical candidate earthquake in southern California for which the causative fault remains unknown and that is of sufficiently large magnitude to be compatible with the large slip observed at the west Piru site (Toppozada *et al.*, 1981; Ellsworth, 1990). Thus, if the surface rupture observed in the west Piru trench occurred during historical time, then it must be the 21 December 1812 event. Ruling out the possibility that this event occurred after 1812 reduces the potential calendric age ranges of samples SCL-40 and -44 to A.D. 1660–1813 and 1641–1813, respectively. We can therefore narrow the potential dates of occurrence of the west Piru trenc event to 1660–1813.

The large magnitude of the paleoseismologically d fined west Piru surface rupture, coupled with its locatic either within, or just to the east of, the zone of major damag during the 21 December event, raises an obvious questio was the eastern San Cayetano fault the source of the 21 De cember 1812 earthquake? First of all, as discussed abov the west Piru surface rupture could have occurred at any tim during the century preceding the historic era. Thus, the pa leoseismologic data cannot be used to show unequivocall that the west Piru surface rupture was the 21 Decembe earthquake. We can, however, discuss whether the west Pir trench data are compatible with the available data concern ing the 21 December 1812 rupture.

The magnitude of the 21 December event, which is gen erally thought to have been in excess of *M* 7 (Toppozada *e al.*, 1981; Ellsworth, 1990), is certainly compatible with th large surface slip observed in the west Piru trench. On th basis of felt-intensity reports, however, the 21 Decembe earthquake has previously been interpreted as having oc curred on an offshore fault beneath the Santa Barbara Chan nel (Toppozada *et al.*, 1981).

A tsunami affected more than 90 km of the coast near Santa Barbara following the 21 December earthquake, with a maximum run-up height of more than 2.5 m (Toppozada *et al.*, 1981; Lander *et al.*, 1993). The leading depression wave reported by eyewitnesses led Lander *et al.* (1993) to suggest that the tsunami was generated by an underwater landslide triggered by strong ground shaking during the earthquake. A submarine landslide source for the tsunami indicates that the earthquake need not have been generated by an offshore fault. Recent side-scan sonar imaging has identified a large (10.5 km wide, 14 km long) submarine landslide off Coal Oil Point in Goleta, ca. 20 km west of Santa Barbara (Greene *et al.*, 2000). This landslide comprises three major sublandslides which may have failed independently of one another. Hydrodynamic modeling of the Coal Oil Point submarine landslide shows that any of the three major sublandslides could have generated the 21 December 1812 tsunami reported along the Santa Barbara coast (Borrero *et al.*, 2001). However, although the location and large size of this landslide make it an attractive candidate to explain the 21 December 1812 tsunami, no age data are currently available from the slide itself. In the absence of such age control, the causative relationship between the Coal Oil Point submarine landslide and the 21 December tsunami must remain somewhat speculative.

One of the more interesting aspects of the modified Mercalli intensity (MMI) maps developed from historical accounts of the earthquake is the apparently abrupt decrease in intensity experienced at Mission La Purisima Concepcion (MMI 8) relative to the nearby Rancho San Antonio, where buildings similar to those heavily damaged at the mission suffered no damage (Toppozada *et al.*, 1981). As noted at the time of the earthquake by the mission padres themselves,

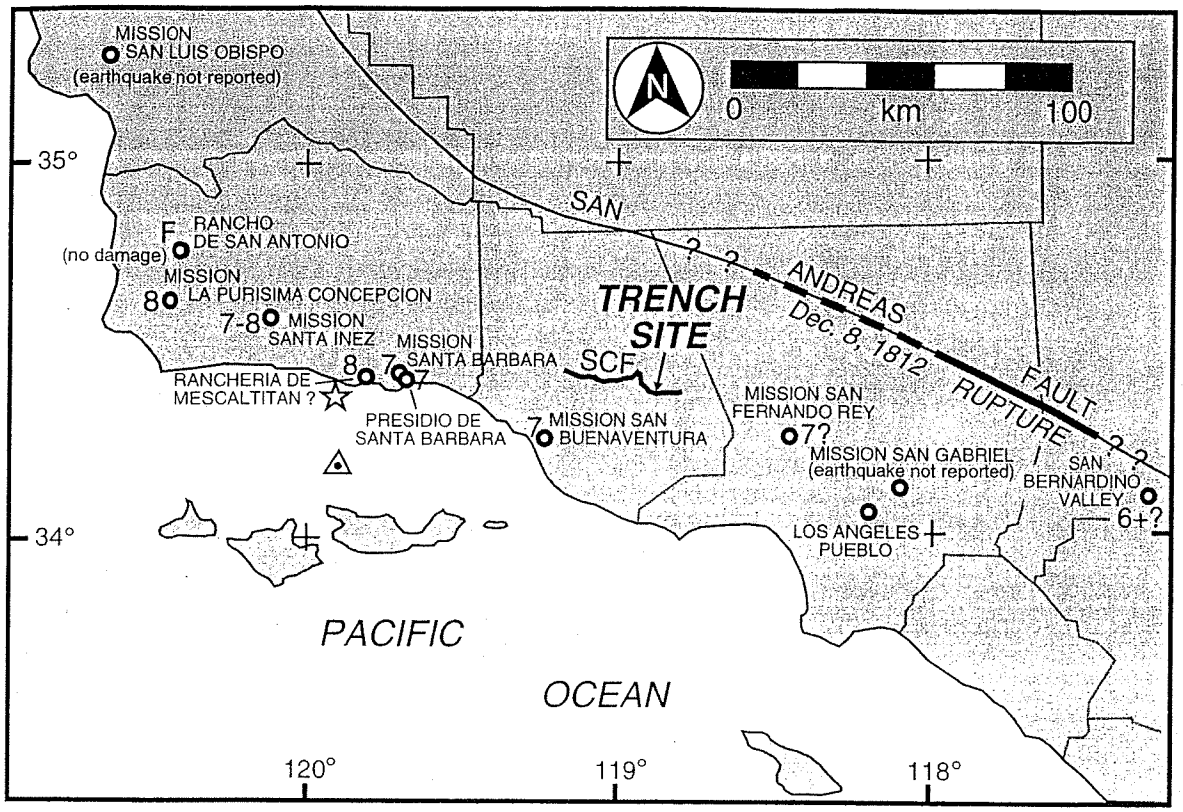

Figure 8. Location map of areas affected by the 21 December 1812 earthquake showing MMI values (from Toppozada *et al.*, 1981). Also shown are the surface traces of the San Andreas and San Cayetano faults, the approximate limits of the 8 December 1812 rupture (Jacoby *et al.*, 1988; Grant, 1996), and the location of the west Piru trench site along the eastern part of the San Cayetano fault. The San Cayetano fault trace is shown for reference only and is not intended to imply the source dimensions of the 21 December 1812 event (see Discussion section). Site of submarine landslide that may have been generated by a tsunami (Greene, 2000; Borrero *et al.*, 2001) during this event is shown by a star. Spanish missions and towns that were extant in 1812 are shown by open circles. Triangle offshore Santa Barbara shows tentative location assigned to the 21 December 1812 event by Toppozada *et al.* (1981). Irregular gray lines onshore denote modern county boundaries.

site effects appear to have played a major role in the extensive damage suffered at the mission. Mission buildings sited on level ground apparently suffered little to no damage, in contrast with other mission buildings that were sited on marshy or sloping ground (Toppozada *et al.*, 1981; T. Toppozada, 2000, personal comm.). These observations suggest the possibility that the actual MMI of the area around the La Purisima mission, away from the marshy ground near the mission, is probably much lower than the maximum MMI 8 reported by Toppozada *et al.* (1981). Decreasing the MMI assigned to the La Purisima area to account for site effects would serve to shift the center of the region of strong ground shaking during the 21 December event somewhat to the east, closer to the San Cayetano fault. Moreover, as noted above, it remains unclear whether the "strong and repeated earthquakes" recorded at mission San Fernando include the mainshock and aftershocks of the 21 December event. If this event was strongly felt at San Fernando, then the area of strong ground shaking during the 21 December event would encompass the epicentral region of the west Piru surface rupture.

Deng and Sykes (1997) modeled the changes in the Coulomb failure function (CFF) in southern California caused by the 8 December 1812 SAF rupture. Their modeling shows that the 8 December event caused a significant, positive increase in CFF (i.e., driving faults closer to failure) for west-striking thrust faults throughout much of the western Transverse Ranges. The area of positive CFF change that they modeled encompasses both the west Piru trench site and the Santa Barbara Channel location postulated by previous workers as the epicenter of the 21 December 1812 earthquake (Fig. 8). Although both sites are located within regions of positive CFF change modeled by Deng and Sykes (1997), the positive CFF change at the west Piru site is much larger than the CFF change at the Santa Barbara Channel site, consistent with the idea that the 8 December 1812 earth-

quake triggered a large earthquake on the eastern San Cayetano fault on 21 December 1812.

To sum up, although the paleoseismologic data from the west Piru trench cannot be used to show definitively that the post-A.D. 1660 surface rupture exposed in the trench is the 21 December 1812 event, the historical observations of the earthquake are compatible with a source on the San Cayetano fault. Moreover, the presence of a weak, buried soil within Unit 4 suggests a time of occurrence for the most recent surface rupture late during the A.D. 1660–1813 time span allowed by the ^{14}C detrital charcoal age from Unit 5. This inference is supported by the lack of any discernible soil development on top of the event horizon in the west Piru trench, although it is possible in such an environment to strip the delicate, weakly developed soils. Finally, the west Piru site is located in a region where the change in CFF following the 8 December 1812 earthquake was both large and positive (Deng and Sykes, 1997).

It is interesting to speculate about the origin of the two major events in the 21 December 1812 sequence. The apparently similar size of the two events, as suggested by the historical accounts from Mission La Purisima, Santa Inez, and Santa Barbara, raises the possibility that they may have been two separate mainshocks, or perhaps a mainshock and a related, triggered event. Among the many possible scenarios that can explain these observations, we suggest one speculative, but plausible, scenario. If the surface rupture observed in the west Piru trench is the 21 December event, one possible cause of the double event could be the rupture of either the eastern or the western lobe of the San Cayetano fault, possibly together with the adjacent faults (e.g., the Santa Susana fault to the east) up to the major lateral fault step at Sespe Creek near Fillmore, followed 15 min later by the second, triggered event on the other lobe. This lateral step is ca. 4 km wide at the surface, and subsurface well data indicate that it extends to at least the 4-km maximum depth of the wells, with no signs of narrowing with depth (Çemen, 1977, 1989). Such major lateral steps along reverse faults have been observed to stop a number of major ruptures (e.g., 1971 M_w 6.7 San Fernando; 1999 M_w 7.6 Chi-Chi, Taiwan). Moreover, recent computer modeling suggests that major lateral steps may act as barriers to rupture propagation (Magistrale and Day, 1999). In the absence of any paleoseismologic data from the western San Cayetano fault, however, this suggestion remains speculative.

Implications for Seismic Hazard in Southern California

The paleoseismologic observations discussed previously indicate that the most recent surface rupture on the eastern San Cayetano fault was larger than M_w 7, and probably closer to M_w 7.5-well in excess of the M_w 6.8 maximum magnitude used in the current State of California probabilistic seismic hazard assessment (Petersen *et al.*, 1996), but similar to the estimates of Rockwell (1988) and Dolan *et al.* (1995). The occurrence of such a large earthquake on the San Cayetano fault should not come as a surprise. During the twentieth century, many reverse faults similar to the San Cayetano fault elsewhere in the world have generated earthquakes considerably larger than M 7 (e.g., 1964 M_s 7.5 Niigata, Japan [Kawasumi, 1973; Satake and Abe, 1983; Okamura *et al.*, 1994]; 1978 M_s 7.4 Tabas-e-Golshan, Iran [Berberian, 1979; Hartzell and Mendoza, 1991; Berberian and Yeats, 1999]; 1980 M_w 7.3 El Asnam, Algeria [King and Vita-Finzi, 1981; Philip and Meghraoui, 1983; Swan, 1988]; 1992 M_w 7.4 Suusamyr, Kyrgyzstan [Ghose *et al.*, 1997; Mellors *et al.*, 1997]; and 1999 M_w 7.6 Chi-Chi, Taiwan [Bilham and Yu, 2000; Shin *et al.*, 2000]). Moreover, the paleoseismologic data from the west Piru trench add to a growing body of evidence that indicates that such large events could occur on reverse faults directly beneath or adjacent to the Los Angeles metropolitan region (e.g., Dolan *et al.*, 1995; Rubin *et al.*, 1998; Shaw and Shearer, 1999; Tucker and Dolan, 2001). Thus, the occurrence of such large events must be considered in all future seismic hazard assessments of the region. Although such events may be somewhat smaller than the large-to-great earthquakes on the SAF, the proximity of large faults such as the San Cayetano fault to the metropolitan region indicates that the major earthquakes generated by these faults could cause at least as much, if not more, damage than a larger event on the more distant SAF.

In the case of the San Cayetano fault, source directivity in future events could play a major role in determining damage patterns. For example, if a major San Cayetano fault rupture were to exhibit strong westward directivity, then much of the seismic energy would be directed toward the communities of the Ventura-Santa Barbara area, but directly away from the much more densely populated Los Angeles metropolitan region (Fig. 1). In contrast, if a large San Cayetano fault event were to exhibit significant eastward directivity, then much of the energy would be directed toward the Los Angeles region. Furthermore, a major surface rupture on the San Cayetano fault would likely excite strong, long-period surface waves (e.g., Liu and Heaton, 1984; Vidale and Helmberger, 1988; Olsen and Archuleta, 1996). Such long-period surface waves could represent a significant hazard to the many high-rise buildings in the Los Angeles metropolitan region (Heaton *et al.*, 1995; Olsen and Archuleta, 1996).

Finally, the late Quaternary average slip rate for the eastern San Cayetano fault is ca. 1 cm/yr (Huftile and Yeats, 1995a), indicating that the 4.3–5.2 m of surface slip generated by the most recent surface rupture exposed in the west Piru trench should recur, on an average, about once every 400–500 yr. If the recurrence of such events is quasi-periodic, and if the surface rupture exposed in the west Piru trench is the 21 December 1812 event, then the relatively brief, 178-yr-long elapsed time interval since that surface rupture suggests that the conditional probability of the recurrence of such an event within the next few decades is relatively low. In contrast, if the most recent surface rupture

at the west Piru site actually occurred during the prehistoric era, near the beginning of the allowable A.D. 1660–1813 age range, then the elapsed greater than 300-yr-long time interval since the earthquake would suggest a much higher conditional probability for the recurrence of such an event.

Conclusions

The first paleoseismologic data from the eastern San Cayetano fault, a major reverse fault located northwest of the Los Angeles metropolitan region, indicate that the fault ruptured to the surface during a very large (M_w >7), recent earthquake. A combination of paleoseismologic and historical data constrain this event, which resulted in at least 4.3 m of reverse slip at our trench site, to have occurred between A.D. 1660 and 1813. The large magnitude of this event, as deduced from the large amount of surface slip, combined with its location, lead us to speculate that it may have been the damaging 21 December 1812 event. This is the largest historical California earthquake for which the causative fault has not yet been determined. The paleoseismologic age constraints, however, cannot be used to confirm this suggestion, and the resolution of the exact timing of the most recent event on the eastern San Cayetano fault event awaits further excavations. Nevertheless, our trench observations add to a growing body of evidence that indicates that major (M_w >7) earthquakes have occurred on faults in and around the metropolitan Los Angeles region. Such large events are much larger than any earthquakes that have occurred on faults within the metropolitan region during the past 150 yr, and seismic hazard analyses must incorporate the occurrence of such large earthquakes directly beneath the metropolitan region.

Acknowledgments

We thank Allan Tucker, Shari Christofferson, Scott Lindvall, Tim Dawson, Marcos Marin, and Jenn Holsten for their help with the excavations. Special thanks are due to Bob Yeats for many helpful discussions regarding the San Cayetano fault. We also thank Tousson Toppozada and Jerry Treiman for helpful discussions. Katherine Kendrick and Tim Dawson provided constructive reviews of the manuscript. We are grateful to Marcos Marin for help with drafting of the figures. This research was supported by the National Earthquake Hazards Reduction Program (NEHRP) of the U.S. Geological Survey, NEHRP Grant Number 1434-HQ-96-GR0273.

References

Argus, D. F., M. B. Heflin, A. Donnellan, F. H. Webb, D. Dong, K. J. Hurst, D. C. Jefferson, G. A. Lyzenga, M. M. Watkins, and J. F. Zumberge (1999). Shortening and thickening of metropolitan Los Angeles measured and inferred using geodesy, *Geology* **27,** 703–706.

Berberian, M. (1979). Earthquake faulting and bedding thrust associated with the Tabas-e-Golshan (Iran) earthquake of September 16, 1978, *Bull. Seism. Soc. Am.* **69,** 1861–1887.

Berberian, M., and R. S. Yeats (1999). Patterns of historical earthquake rupture in the Iranian Plateau, *Bull. Seism. Soc. Am.* **89,** 120–139.

Bilham, R., and T.-T. Yu (2000). The morphology of thrust faulting in the 21 September 1999, Chichi, Taiwan earthquake, *J. Asian Earth Sci.* **18,** 351–367.

Borrero, J. C., J. F. Dolan, and C. E. Synolakis (2001). Tsunamis within the eastern Santa Barbara Channel, *Geophys. Res. Lett.* **28,** 643–646.

Bryant, A. S., and L. M. Jones (1992). Anomalously deep earthquakes in the Ventura Basin, southern California, *J. Geophys. Res.* **97,** 437–447.

Çemen, I. (1977). Geology of the Sespe-Piru Creek area, Ventura County, California, *Master's Thesis,* Ohio University, Athens, 69 pp.

Çemen, I. (1989). Near-surface expression of the eastern part of the San Cayetano fault: a potentially active thrust fault in the California Transverse Ranges, *J. Geophys. Res.* **94,** 9665–9677.

Deng, J., and L. R. Sykes (1997). Evolution of the stress field in southern California and triggering of moderate-size earthquakes, *J. Geophys. Res.* **102,** 9859–9886.

Dibblee Jr., T. W. (1987). Geologic map of the Ojai Quadrangle, Ventura County, California: Dibblee Geological Foundation map #DF-13, Santa Barbara, California, scale 1:24,000.

Dibblee Jr., T. W. (1990a). Geologic map of the Fillmore Quadrangle, Ventura County, California: Dibblee Geological Foundation map #DF-27, Santa Barbara, California, scale 1:24,000.

Dibblee Jr., T. W. (1990b). Geologic map of the Santa Paula Peak Quadrangle, Ventura County, California: Dibblee Geological Foundation map #DF-26, Santa Barbara, California, scale 1:24,000.

Dibblee Jr., T. W. (1991). Geologic map of the Piru Quadrangle, Ventura County, California: Dibblee Geological Foundation map #DF-34, Santa Barbara, California, scale 1:24,000.

Dolan, J. F., and K. Sieh (1992). Tectonic geomorphology of the northern Los Angeles basin: seismic hazards and kinematics of young fault movement, in *Engineering Geology Field Trips: Orange County, Santa Monica Mountains, and Malibu, Guidebook and Volume,* P. L. Ehlig and E. A. Steiner (Editors), Association of Engineering Geologists, Los Angeles, California, B-20-B-26.

Dolan, J. F., K. Sieh, and T. K. Rockwell (2000). Late Quaternary activity and seismic potential of the Santa Monica fault system, Los Angeles, California, *Geol. Soc. Am. Bull.* **112,** 1559–1581.

Dolan, J. F., K. Sieh, T. K. Rockwell, P. Guptill, and G. Miller (1997). Active tectonics, paleoseismology, and seismic hazards of the Hollywood fault, northern Los Angeles basin, California, *Bull. Geol. Soc. Am.* **109,** 1595–1616.

Dolan, J. F., K. Sieh, T. K. Rockwell, R. S. Yeats, J. Shaw, J. Suppe, G. Huftile, and E. Gath (1995). Prospects for larger or more frequent earthquakes in greater metropolitan Los Angeles, California, *Science* **267,** 199–205.

Donnellan, A., B. H. Hager, and R. W. King (1993a). Rapid north-south shortening of the Ventura basin, southern California, *Nature* **366,** 333–336.

Donnellan, A., B. H. Hager, R. W. King, and T. A. Herring (1993b). Geodetic measurement of deformation in the Ventura basin, southern California, *J. Geophys. Res.* **98,** 21,727–21,739.

Ellsworth, W. L. (1990). Earthquake history, 1769–1989, in *The San Andreas Fault System,* R. E.Wallace (Editor), *U.S. Geol. Surv. Profess. Pap. 1515,* 153–187.

Ghose, S., R. J. Mellors, A. M. Korjenkov, M. W. Hamburger, T. L. Pavlis, G. L. Pavlis, M. Omuraliev, E. Mamyrov, and Muraliev (1997). The M_s = 7.3 1992 Suusamyr, Kyrgyzstan, earthquake in the Tien Shan: 2. Aftershock focal mechanisms and surface deformation, *Bull. Seism. Soc. Am.* **87,** 23–38.

Grant, L. B. (1996). Uncharacteristic earthquakes on the San Andreas fault, *Science* **272,** 826–827.

Greene, H. G., N. Maher, and C. K. Paull (2000). Landslide hazards off of Santa Barbara, California (abstract), *EOS* **81,** F-750.

Hartzell, S., and C. Mendoza (1991). Application of an iterative least-squares waveform inversion of strong-motion and teleseismic records to the 1978 Tabas, Iran, earthquake, *Bull. Seism. Soc. Am.* **81,** 301–335.

Heaton, T. H., J. F. Hall, D. J. Wald, and M. W. Halling (1995). Response of high-rise and base-isolated buildings to a hypothetical M_w 7.0 blind thrust earthquake, *Science* **267,** 206–211.

Huftile, G. J., and R. S. Yeats (1995a). Convergence rates across a displacement transfer zone in the western Transverse Ranges, Ventura Basin, California, *J. Geophys. Res.* **100,** 2043–2067.

Huftile, G. J., and R. S. Yeats (1995b). Cenozoic structure of the Piru 7½-minute quadrangle, California, *U.S. Geol. Surv. Open-File Rept. 95–68,* map scale 1:24,000, 33 pp.

Huftile, G. J., and R. S. Yeats (1996). Deformation rates across the Placerita (Northridge M_w 6.7 aftershock zone) and Hopper Canyon segments of the western Transverse Ranges deformation belt, *Bull. Seism. Soc. Am.* **86,** S3-S18.

Jacoby, G. C., P. R. Sheppard, and K. E. Sieh (1988). Irregular occurrence of large earthquakes along the San Andreas fault: evidence from trees, *Science* **241** 196–199.

Kawasumi, H. (Editor) (1973). *General Report on the Niigata Earthquake of 1964,* Tokyo Electrical Engineering College Press, Tokyo.

King, G. C. P., and C. Vita-Finzi (1981). Active folding in the Algerian earthquake of 10 October 1980, *Nature* **292,** 22–26.

Lander, J. F., P. A. Lockridge, and M. J. Kozuch (1993). *Tsunamis Affecting the West Coast of the United States 1806–1992,* U.S. Department of Commerce, NOAA, 242 pp.

Liu, H., and T. Heaton (1984). Ray analysis of ground velocities and accelerations from the 1971 San Fernando, California, earthquakes, *Bull. Seism. Soc. Am.* **74,** 1951–1968.

Magistrale, H., and S. Day (1999). 3-D simulations of multi-segment thrust fault rupture, *Geophys. Res. Lett.* **26,** 2093–2096.

Mellors, R. J., F. L. Vernon, G. L. Pavlis, G. A. Abers, M. W. Hamburger, S. Ghose, and B. Iliasov (1997). The M_s = 7.3 1992 Suusamyr, Kyrgyzsatn, earthquake: 1. Constraints on fault geometry and source parameters based on aftershocks and body-wave modeling, *Bull. Seism. Soc. Am.* **87,** 11–22.

Namson, J., and T. Davis (1988). Structural transect of the western Transverse Ranges, California: implications for lithospheric kinematics and seismic risk evaluation, *Geology* **16,** 675–679.

Okamura, Y., M. Satoh, and J. Miyazaki (1994). Active faults and folds on the shelf off Niigata and their relation to the 1964 Niigata earthquake, *J. Seism. Soc. Jpn.* **46,** 413–423 (in Japanese with English abstract).

Olsen, K. B., and R. J. Archuleta (1996). Site response in the Los Angeles basin from 3-D simulations of ground motion (abstract), *Seism. Res. Lett.* **67,** 49.

Petersen, M. D., W. D. Bryant, C. H. Cramer, T. Cao, M. S. Reichle, A. D. Frankel, J. J. Lienkamper, P. A. McCrory, and D. P. Schwartz (1996). Probabilistic seismic hazard assessment for the state of California, *Calif. Div. Mines Geol. Open File 96–08 and U.S. Geol. Surv. Open-File Rept. 96–706.*

Philip, H., and M. Meghraoui (1983). Structural analysis and interpretation of the surface deformation of the El Asnam earthquake of October 10, 1980, *Tectonics* **2,** 17–49.

Rockwell, T. (1988). Neotectonics of the San Cayetano fault, Transverse Ranges, California, *Geol. Soc. Am. Bull.* **100,** 500–513.

Rockwell, T. K., D. L. Johnson, E. A. Keller, and G. R. Dembroff (1985). A late Pleistocene-Holocene soil chronosequence in the central Ventura Basin, southern California, USA, in *Geomorphology and Soils,* K. Richards, R. Arnette and S. Ellis (Editors), George Allen and Unwin, London, 309–327.

Rubin, C., S. Lindvall, and T. K. Rockwell (1998). Evidence for large earthquakes in metropolitan Los Angeles, *Science* **281,** 398–402.

Satake, K., and K. Abe (1983). A fault model for the Niigata, Japan, earthquake of June 16, 1964, *J. Phys. Earth* **31,** 217–223.

Schleuter, J. C. (1976). Structure of the Upper Ojai-Timber Canyon area, Ventura County, California, *Master's Thesis,* Ohio University, 67 pp.

Shaw, J. H., and P. M. Shearer (1999). An elusive blind thrust fault beneath metropolitan Los Angeles, *Science* **283,** 1516–1518.

Shaw, J. H., and J. Suppe (1996). Earthquake hazards of active blind thrust faults under the central Los Angeles Basin, California, *J. Geophys. Res.* **101,** 8623–8642.

Shin, T. C., K. W. Kuo, W. H. K. Lee, T. L. Teng, and Y. B. Tsai (2000). A preliminary report on the 1999 Chi-Chi (Taiwan) earthquake, *Seism. Res. Lett.* **71,** 24–30.

Sorlien, C. C. (1994). Faulting and uplift of the northern Channel Islands, California, in *Proceedings, Fourth Channel Islands Symposium: Update on the Status of Resources,* W. L. Halvorson and G. J. Maender (Editors), Santa Barbara County Museum of Natural History, Santa Barbara, California, 281–296.

Stuiver, M., and P. J. Reimer (1993). Radiocarbon calibration program revision 4.3 for MacIntosh, *Radiocarbon* **35,** 215–230.

Suppe, J., and D. A. Medwedeff (1990). Geometry and kinematics of fault-propagation folding, *Ecologae Geol. Helvetica* **83,** 409–454.

Swan, F. H. (1988). Temporal clustering of paleoseismic events on the Oued Fodda fault, Algeria, *Geology* **16,** 1092–1095.

Toppozada, T. R., C. R. Real, and D. L. Parke (1981). Preparation of isoseismal maps and summaries of reported effects for pre-1900 California earthquakes, *Calif. Div. Mines Geol. Open-File Rept. 81–11,* Sacramento, California.

Tucker, A. Z., and J. F. Dolan (2001). Paleoseismologic evidence for a >8 ka age for the most recent surface rupture on the eastern Sierra Madre fault, northern Los Angeles metropolitan region, *Bull. Seism. Soc. Am.* **91,** 232–249.

Vedder, J. G., H. G. Greene, S. H. Clarke, and M. P. Kennedy (1986). Geologic map of mid-southern California continental margin (Map 2A), California continental margin geologic map series (area 2 of 7; map sheet 1 of 4), scale 1:250,000, H. Greene and M. Kennedy (Editors), U.S. Geol. Survey, Menlo Park, California, and Calif. Div. Mines Geol., Sacramento, California.

Vidale, J. E., and D. V. Helmberger (1988). Elastic finite-difference modeling of the 1971 San Fernando California earthquake, *Bull. Seis. Soc. Am.* **78,** 122–141.

Wells, D., L., and K. L. Coppersmith (1994). New empirical relationships among magnitude, rupture length, rupture width, rupture area, and surface displacement, *Bull. Seism. Soc. Am.* **84,** 974–1002.

Yeats, R. S. (1987). Late Cenozoic structure of the Santa Susana fault zone, *U.S. Geol. Surv. Profess. Pap. 1339,* 137–160.

Yeats, R. S. (1993). Converging more slowly, *Nature* **366,** 299–301.

Yeats, R. S. (2001). Neotectonics of the East Ventura and San Fernando basins, California: an overview, in *Geology and Tectonics of the East Ventura Basin: Geological Society of America Cordilleran Section Field Trip Guidebook,* T. L. Wright and R. S. Yeats (Editors), Universal City, California, 9 April 2001, 9–36.

Yeats, R. S., G. J. Huftile, and L. T. Stitt (1994). Late Cenozoic tectonics of the East Ventura basin, Transverse Ranges, California, *Am. Assoc. Pet. Geol. Bull.* **78,** 1040–1074.

Ziony, J. I., and L. M. Jones (1989). Map showing late Quaternary faults and 1978–84 seismicity of the Los Angeles region, U.S. Geol. Survey Misc. Field Studies Map MF-1964, scale 1:250,000.

Department of Earth Sciences
University of Southern California
Los Angeles, California 90089-0740
dolan@earth.usc.edu
(J.F.D.)

Department of Geology
San Diego State University
San Diego, California 92182
trockwell@geology.sdsu.edu
(T.K.R.)

Manuscript received 10 January 2001.